

# Forecasting the $E_G$ measurements from the photometric and spectroscopic surveys of Chinese Space Station Survey Telescope (CSST)

**Yu Song**<sup>a,b</sup> and **Yi Zheng**<sup>a,b,1</sup>

<sup>a</sup>School of Physics and Astronomy, Sun Yat-sen University, 2 Daxue Road, Tangjia, Zhuhai, 519082, China

<sup>b</sup>CSST Science Center for the Guangdong-Hong Kong-Macau Greater Bay Area, SYSU, Zhuhai, 519082, China

E-mail: [songy67@mail2.sysu.edu.cn](mailto:songy67@mail2.sysu.edu.cn), [zhengyi27@mail.sysu.edu.cn](mailto:zhengyi27@mail.sysu.edu.cn)

**Abstract.** We present forecasts for the  $E_G$  statistic using redshift distributions of realistic mock galaxy samples from the upcoming Chinese Space Station Survey Telescope (CSST). The dominant uncertainty in  $E_G$  stems from the redshift space distortion parameter  $\beta$ , whose precision limits the overall constraining power. Our analysis shows that CSST will nevertheless achieve  $E_G$  constraints at the few-percent level (3% – 9%) over  $0 < z < 1.2$ , an improvement by a factor of several to an order of magnitude over current observations. Within the  $\mu - \Sigma$  modified gravity framework, the parameter  $\Sigma_0$ , associated with the effective gravitational constant of the Weyl potential, can be constrained to  $\sim 5\%$  precision. In a plausible scenario where upcoming spectroscopic surveys determine  $\beta$  to 1% accuracy,  $E_G$  constraints tighten to the percent level, and  $\Sigma_0$  becomes measurable at  $\sim 1\%$ . These results demonstrate that CSST will serve as a powerful facility for testing gravity and underscore the essential synergy between photometric weak lensing and spectroscopic surveys in probing cosmic acceleration.

---

<sup>1</sup>Corresponding author.

---

## Contents

<b>1</b>	<b>Introduction</b>	<b>1</b>
<b>2</b>	<b>Analysis framework</b>	<b>2</b>
2.1	Observational definition of $E_G$	2
2.2	Error propagation and covariance estimation	3
2.3	$\mu-\Sigma$ parameterization for modified gravity	5
<b>3</b>	<b>CSST surveys</b>	<b>6</b>
<b>4</b>	<b>Results</b>	<b>8</b>
4.1	$E_G$ predictions	8
4.2	Constraints on modified gravity	10
<b>5</b>	<b>Conclusion</b>	<b>11</b>

---

## 1 Introduction

Since the discovery of the accelerated expansion of the Universe [1, 2], understanding its physical origin has remained one of the most profound challenges in modern cosmology. Although some observational tensions persist [3–7], the widely accepted  $\Lambda$ CDM model, which incorporates a cosmological constant to drive acceleration, agrees well with a broad range of observations [8–13]. However, the theoretical puzzles associated with the cosmological constant, most notably the fine-tuning and coincidence problems [14, 15], motivate the exploration of alternative explanations. These include dynamical dark energy models, which introduce a time-varying component, and modifications to General Relativity (GR) on cosmological scales [16, 17]. Many of these models, however, lead to similar observational signatures, creating degeneracies that complicate their distinction through conventional cosmological probes alone [18–20].

In this context, tests of gravity on cosmological scales have become a central focus of next-generation surveys [e.g., 21, 22]. A particularly powerful probe is the  $E_G$  statistic, first introduced by [23]. This quantity is constructed from a combination of galaxy-galaxy lensing and galaxy clustering measurements. Its key strength lies in its independence from galaxy bias and the amplitude of the matter power spectrum  $\sigma_8$  on linear scales, while also benefiting from a partial cancellation of cosmic variance, since both observables trace the same underlying density field. This makes  $E_G$  a robust, nearly model-independent diagnostic for deviations from GR, particularly sensitive to modifications in the relationship between the gravitational potentials and the matter distribution.

Current measurements of  $E_G$  have relative uncertainties mostly in the range of 10% – 35% [24–35], with two outliers reaching  $\sim 56\%$  and 78% [36]. While these results are generally consistent with GR, they are still limited by statistical power and systematic uncertainties. The next generation of wide-field imaging and spectroscopic surveys, such as Euclid [37], LSST [38], DESI [39] and PFS [40] et al., are designed to deliver order-of-magnitude improvements in data volume and depth. In particular, China’s upcoming Chinese Space Station

Survey Telescope (CSST) will perform a deep, multi-band photometric and slitless spectroscopic survey over approximately  $17,500 \text{ deg}^2$  [41]. Its unique combination of high-quality imaging and spectroscopic redshift measurements makes it exceptionally well suited for precise  $E_G$  estimation, enabling tomographic gravity tests across a broad redshift range.

In this work, we present forecasts for the constraining power of CSST on the  $E_G$  statistic. We develop a harmonic-space covariance framework that fully accounts for correlations between galaxy-galaxy lensing and galaxy clustering observables, and we employ realistic mock galaxy samples to model the expected redshift distributions and number densities of the CSST photometric and spectroscopic surveys. Our analysis quantifies the statistical precision attainable on  $E_G$  as a function of scale and redshift, identifies the dominant sources of uncertainty, and translates the forecasts into constraints on phenomenological modified gravity parameters within the widely used  $\mu - \Sigma$  parametrization [42].

The paper is organized as follows: Section 2 outlines the theoretical and observational definitions of  $E_G$ , the error propagation methodology, and the modified gravity parameterization. Section 3 describes the survey specifications of CSST and the mock galaxy samples used in our forecasts. Section 4 presents the predicted  $E_G$  measurements and their statistical uncertainties, as well as the resulting constraints on modified gravity parameters. Finally, Section 5 summarizes our conclusions and discusses future prospects.

## 2 Analysis framework

The  $E_G$  statistic combines cosmological weak lensing and galaxy clustering observations to probe the relationships between Bardeen potentials and the matter density fluctuation  $\delta$ , where Bardeen potentials  $\Psi$  and  $\Phi$  are potential perturbations in the perturbed Friedmann Robertson Walker (FRW) metric  $d\tau^2 = (1 + 2\Psi)dt^2 - a^2(1 - 2\Phi)d\mathbf{x}^2$ .

In Fourier space, the theoretical definition of  $E_G$  can be expressed as [23]:

$$E_G(k, z) = \frac{c^2 k^2 (\Psi - \Phi)}{3H_0^2(1 + z)\theta(k)}, \quad (2.1)$$

where  $H_0$  is the Hubble constant, and  $\theta(k)$  is the divergence of the peculiar velocity field. On linear scales,  $\theta(k) = f(z)\delta(k)$ , with  $f(z)$  being the linear structure growth rate.

In the context of GR,  $\Psi = \Phi$ , the theoretical expectation of  $E_G$  can be simplified using the Poisson equation, yielding:

$$E_G(z) = \frac{\Omega_{m,0}}{f(z)}, \quad (2.2)$$

where  $\Omega_{m,0}$  is the density parameter of the matter at the present day, and  $f(z) \approx [\Omega_m(z)]^\gamma$  with  $\gamma = 0.55$  for GR [43].

### 2.1 Observational definition of $E_G$

The next generation of weak lensing surveys will provide about ten times larger sky coverage than current ones [41, 44, 45], which is ideal for harmonic-space statistics. This expansion, combined with the growing maturity of accurate  $\kappa$  reconstruction methods for masked shear catalog [46], enhances the practical benefits of power spectrum analysis, including easier theoretical modeling and covariance estimation, among others. Consequently, we focus this work on harmonic-space forecasts for  $E_G$ .

Under the Limber approximation, the angular power spectra of galaxy-galaxy lensing ( $C_\ell^{g\kappa}$ ) and galaxy clustering ( $C_\ell^{gg}$ ) can be written as follows:

$$C_\ell^{g\kappa} = \int dz f_g(z) \frac{H(z)}{c} W_\kappa(z) \chi^{-2}(z) P_{\delta g} \left( k = \frac{\ell + 1/2}{\chi(z)}, z \right), \quad (2.3)$$

$$C_\ell^{gg} = \int dz f_g^2(z) \frac{H(z)}{c} \chi^{-2}(z) P_{gg} \left( k = \frac{\ell + 1/2}{\chi(z)}, z \right), \quad (2.4)$$

where  $f_g(z)$  is the galaxy redshift distribution,  $\chi(z)$  is the comoving distance to redshift  $z$ , and  $\ell$  is the multipole moment. The lensing kernels is defined respectively as:

$$W_\kappa(z, z_s) = \frac{3H_0^2 \Omega_{m,0}}{2c^2} (1+z) \chi(z) \left[ 1 - \frac{\chi(z)}{\chi(z_s)} \right], \quad (2.5)$$

where  $z_s$  is the source redshift, and  $dN/dz$  is the normalized redshift distribution of the lens galaxies. The galaxy clustering traces the underlying matter distribution with a scale-independent linear bias on large scales, such that:  $P_{\delta g} = b_g P_{\delta\delta}$ ,  $P_{gg} = b_g^2 P_{\delta\delta}$ .

The observational definition of  $E_G(\ell)$  can then be expressed in Harmonic space as [47]:

$$\hat{E}_G(\ell) = \Gamma(\ell, z) \frac{C_\ell^{g\kappa}}{\beta C_\ell^{gg}}, \quad (2.6)$$

where

$$\Gamma(\ell, z) = \frac{2c}{3H_0} \left[ \frac{f_g(z) H(z)}{W_\kappa(z)(1+z) H_0} \right] \quad (2.7)$$

is a scale-independent prefactor related to lensing efficiency and geometric factors. This formulation allows for a scale-dependent and tomographic estimation of  $E_G$ , suitable for the joint galaxy-galaxy lensing and galaxy clustering analyses.

The redshift space distortion (RSD) parameter  $\beta$  is defined as  $\beta = f(z)/b_g$ . At linear scales,  $b_g$  and  $P_{\delta\delta}$  consequently cancel out in equation (2.6), rendering the  $E_G$  statistic independent of both galaxy bias and the matter power spectrum amplitude. As a result, measurements of (or marginalization over)  $b_g$  and  $\sigma_8$ , which are typically required in other gravity probes, become unnecessary.

## 2.2 Error propagation and covariance estimation

In this study, we adopt a systematic error propagation framework to evaluate the measurement uncertainties of the  $E_G$  statistic. This framework is constructed based on the observed ratio of angular power spectra, fully accounting for the statistical correlations between the galaxy-convergence cross-power spectrum and the galaxy auto-power spectrum. It provides a reliable foundation for uncertainty estimation of  $E_G$  in cosmological interpretation.

We first define the observed ratio of angular power spectra as:

$$\mathcal{R}(\ell) \equiv \frac{C_\ell^{g\kappa}}{C_\ell^{gg}}. \quad (2.8)$$

A key advantage of the  $E_G$  estimator is the cancellation of cosmic variance at large scales, since both  $C_\ell^{g\kappa}$  and  $C_\ell^{gg}$  are sourced by the same underlying density field. Despite this benefit, their strong positive correlation complicates the covariance estimation. As shown

later, we explicitly incorporate the full covariance between  $C_\ell^{g\kappa}$  and  $C_\ell^{gg}$  in our analysis, to ensure accurate error propagation.

Based on this definition, the  $E_G$  statistic in harmonic space can be reexpressed from equation (2.6) as:

$$E_G(\ell) = \mathcal{R}(\ell) \frac{\Gamma}{\beta}, \quad (2.9)$$

and its covariance approximately satisfies:

$$\frac{\text{Cov}[E_G(\ell)E_G(\ell')]}{E_G(\ell)E_G(\ell')} = \frac{\text{Cov}[\mathcal{R}(\ell)\mathcal{R}(\ell')]}{\mathcal{R}(\ell)\mathcal{R}(\ell')} + \frac{\sigma^2[\beta]}{\beta^2}, \quad (2.10)$$

where  $\mathcal{R}(\ell)$  and  $\beta$  are assumed to have statistically independent errors. This relation shows that the uncertainty in  $E_G$  can be decomposed into two contributions: the measurement error of the power-spectrum ratio and that of the RSD parameter.

Therefore, the construction of the covariance matrix of  $\mathcal{R}(\ell)$  is a key component of the uncertainty analysis. Based on the theory of multivariate Gaussian random fields, and including possible non-Gaussian correction terms, the full covariance expression is:

$$\begin{aligned} \text{Cov}[\mathcal{R}(\ell), \mathcal{R}(\ell')] &= \frac{1}{C_{gg}(\ell)C_{gg}(\ell')} \text{Cov}[C_{g\kappa}(\ell), C_{g\kappa}(\ell')] \\ &+ \frac{C_{g\kappa}(\ell)C_{g\kappa}(\ell')}{C_{gg}^2(\ell)C_{gg}^2(\ell')} \text{Cov}[C_{gg}(\ell), C_{gg}(\ell')] \\ &- \frac{C_{g\kappa}(\ell')}{C_{gg}^2(\ell')} \frac{1}{C_{gg}(\ell)} \text{Cov}[C_{g\kappa}(\ell), C_{gg}(\ell')] \\ &- \frac{C_{g\kappa}(\ell)}{C_{gg}^2(\ell)} \frac{1}{C_{gg}(\ell')} \text{Cov}[C_{g\kappa}(\ell'), C_{gg}(\ell)]. \end{aligned} \quad (2.11)$$

In practice, the covariance between two angular power spectra can be expanded as:

$$\text{Cov}[C_{XY}(\ell), C_{ZW}(\ell')] = \frac{\delta_{\ell\ell'}}{(2\ell+1)\Delta\ell f_{\text{sky}}} [C_{XZ}(\ell)C_{YW}(\ell) + C_{XW}(\ell)C_{YZ}(\ell)] + \text{Cov}^{\text{NG}}, \quad (2.12)$$

where the first term represents the Gaussian cosmic variance contribution,  $f_{\text{sky}}$  is the sky coverage fraction, and  $\Delta\ell$  is the multipole bin width. The second term denotes the non-Gaussian connected contribution, which becomes significant in the nonlinear regime.

The Gaussian covariance terms are given by

$$\text{Cov}^{(G)}[C_{g\kappa}(\ell), C_{g\kappa}(\ell')] = \frac{1}{(2\ell+1)\Delta\ell f_{\text{sky}}} \left[ C_{g\kappa}^2(\ell) + \left( C_{gg}(\ell) + \frac{1}{n_g} \right) \left( C_{\kappa\kappa}(\ell) + \frac{\sigma_\gamma^2}{n_s} \right) \right], \quad (2.13)$$

$$\text{Cov}^{(G)}[C_{gg}(\ell), C_{gg}(\ell')] = \frac{1}{(2\ell+1)\Delta\ell f_{\text{sky}}} 2 \left( C_{gg}(\ell) + \frac{1}{n_g} \right)^2, \quad (2.14)$$

$$\text{Cov}^{(G)}[C_{g\kappa}(\ell), C_{gg}(\ell')] = \frac{1}{(2\ell+1)\Delta\ell f_{\text{sky}}} 2 \left( C_{gg}(\ell) + \frac{1}{n_g} \right) C_{g\kappa}(\ell). \quad (2.15)$$

where  $n_g$  and  $n_s$  are the angular number densities of lens and source galaxies, and  $\sigma_\gamma$  is the intrinsic shape noise. The covariance is dominated by: (i) cosmic variance,  $\propto [(2\ell +$

$1)\Delta\ell f_{\text{sky}}]^{-1}$ , at large scales – a contribution that is partially canceled in  $E_G$ ; and (ii) shotnoise ( $\propto 1/n_g$ ) and shape noise ( $\propto \sigma_\gamma^2/n_s$ ) at small scales. The overall signal-to-noise of the  $E_G$  estimator is therefore set by the sky fraction  $f_{\text{sky}}$ , the shape noise  $\sigma_\gamma$ , and the galaxy densities  $n_g$  and  $n_s$ .

The non-Gaussian term arises from the non-Gaussian statistics of the matter density field and can be described by the connected trispectrum:

$$\begin{aligned} \text{Cov}^{\text{cNG}} [C_{XY}(\ell), C_{ZW}(\ell')] \\ = \frac{1}{4\pi f_{\text{sky}}} \int \frac{d\chi}{\chi^6} W_X(\chi) W_Y(\chi) W_Z(\chi) W_W(\chi) T_m\left(\frac{\ell+1/2}{\chi}, \frac{\ell'+1/2}{\chi}, \chi\right), \end{aligned} \quad (2.16)$$

where  $\chi$  is the comoving distance,  $W_X(\chi)$  is the weight function of probe  $X$ , and  $T_m(k_1, k_2, \chi)$  is the three-dimensional connected trispectrum of the matter power spectrum, characterizing the four-point correlations beyond the Gaussian approximation. We evaluate the non-Gaussian covariance part via `pyccl`<sup>1</sup> [48].

The full covariance matrix  $\mathbf{C} = \text{Cov}[E_G(\ell), E_G(\ell')]$  enables a robust scale-dependent analysis of  $E_G(\ell)$  for testing modified gravity theories. To obtain a single, scale-independent constraint, we then combine the measurements across multipole bins using an inverse-variance weighted estimator, yielding

$$\sigma^2(E_G) = (\mathbf{1}^T \mathbf{C}^{-1} \mathbf{1})^{-1}, \quad (2.17)$$

where  $\mathbf{1}$  is the unit vector with a length equal to the number of  $\ell$  bins. This estimator corresponds to a minimum-variance combination of the  $E_G(\ell)$  measurements, ensuring the tightest possible  $E_G$  constraint given the covariance.

The above methodological framework not only provides a solid statistical foundation for the  $E_G$  forecast from the CSST survey, but can also be extended to other next-generation cosmological surveys. By fully accounting for the covariance structure among observables, we can robustly assess the ability of the  $E_G$  statistic to distinguish GR from modified gravity theories, laying the methodological groundwork for future precision tests of gravity.

### 2.3 $\mu-\Sigma$ parameterization for modified gravity

In modified gravity frameworks, departures from GR can be parametrized through modifications of the two metric potentials  $\Psi$  and  $\Phi$  using the functions  $\mu(a, k)$  and  $\Sigma(a, k)$  [42]:

$$k^2 \Psi = -4\pi G a^2 [1 + \mu(k, z)] \rho \delta, \quad (2.18)$$

$$k^2 (\Psi + \Phi) = -8\pi G a^2 [1 + \Sigma(k, z)] \rho \delta. \quad (2.19)$$

Here,  $\mu$  modifies the Newtonian potential responsible for structure growth, while  $\Sigma$  determines the amplitude of the Weyl potential directly probed by lensing.

Under this parametrization, the theoretical prediction of the  $E_G$  statistic can be written as :

$$E_G(k, z) = \frac{\Omega_{m,0} [1 + \Sigma(k, z)]}{2 f(k, z)}. \quad (2.20)$$

In modified gravity scenarios, the linear growth rate  $f(k, z)$  is computed by integrating the modified growth equation with the effective gravitational strength determined by  $\mu(k, z)$  [48].

---

<sup>1</sup><https://github.com/LSSTDESC/CCL>

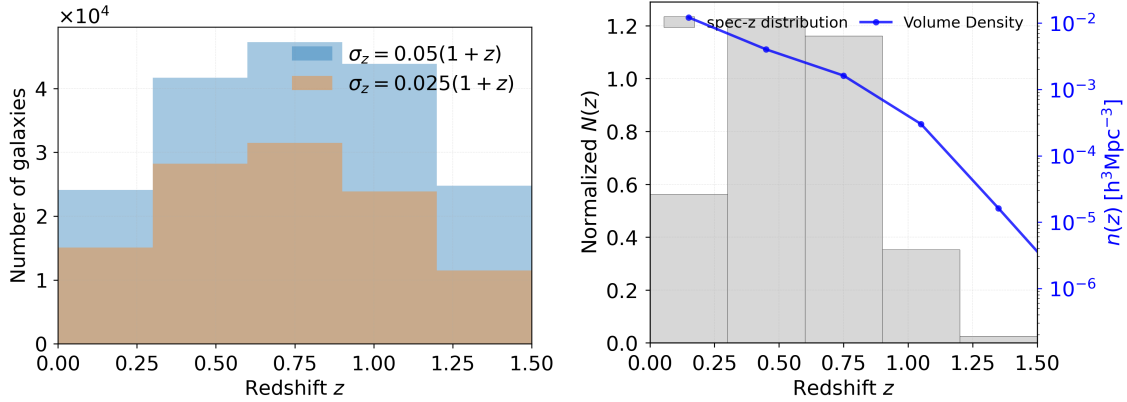


**Figure 1.** *Left:* Redshift distributions of galaxies in the CSST photometric survey. The distributions are derived from a sub-set of the COSMOS catalog within  $1.7 \text{ deg}^2$ . We adopt the  $\sigma_z = 0.025(1+z)$  sample in our analysis. *Right:* Galaxy redshift distribution for the CSST slitless spectroscopic (spec-z) survey. The distribution is normalized following [51], and the comoving number density evolution with redshift is also shown.

For simplicity, in this work we will ignore the scale dependence and adopt phenomenological late-time forms for  $\mu$  and  $\Sigma$ :

$$\mu(z) = \mu_0 \frac{\Omega_\Lambda(z)}{\Omega_\Lambda(0)}, \quad \Sigma(z) = \Sigma_0 \frac{\Omega_\Lambda(z)}{\Omega_\Lambda(0)}, \quad (2.21)$$

which preserve early-universe constraints but allow deviations from GR at low redshift [e.g., 49, 50].

By substituting the solution of the growth equation into equation (2.20), one obtains the theoretical prediction  $E_G^{\text{th}}(z; \mu_0, \Sigma_0)$ , which can be directly compared to observations. By assuming the  $E_G$  measurements of different  $z$  are uncorrelated, the Gaussian likelihood is given by

$$-\ln \mathcal{L} \propto \chi^2(\mu_0, \Sigma_0) = \sum_i \frac{[E_G^{\text{obs}}(z_i) - E_G^{\text{th}}(z_i; \mu_0, \Sigma_0)]^2}{\sigma_{E_G(z_i)}^2}. \quad (2.22)$$

The best-fit values and confidence intervals for  $(\mu_0, \Sigma_0)$  can be obtained by minimizing  $\chi^2$ .

### 3 CSST surveys

CSST is a 2 meter space telescope for the Stage IV dark energy experiment. It will operate in the same orbit as the China Space Station and is designed to perform a high resolution, wide field photometric and spectroscopic survey covering approximately  $17,500 \text{ deg}^2$  of the sky over a 10-year mission duration [41].

The CSST main focal plane is divided into 7 photometric imaging bands (NUV,  $u$ ,  $g$ ,  $r$ ,  $i$ ,  $z$ , and  $y$ ) and 3 slitless spectroscopic bands (GU, GV, and GI), covering the wavelength range of 255–1000 nm with an average spectral resolution of  $R \geq 200$ . The  $17,500 \text{ deg}^2$  slitless spectroscopic wide-field survey is performed simultaneously with the multi-color imaging survey, achieving magnitude limits of not less than 22 mag for the GU band and not less than 23 mag for both the GV and GI bands. [41]

Redshift range	$V_{\text{survey}}$ [ $h^{-3} \text{ Gpc}^3$ ]	$\bar{n}_g$ [ $10^{-4} h^3 \text{ Mpc}^{-3}$ ]	$b_g(z)$	$\sigma(\beta)/\beta$
$0.0 < z < 0.3$	1.03	121.93 (1283.6)	1.126	8.73%
$0.3 < z < 0.6$	5.41	40.18 (456.5)	1.378	4.02%
$0.6 < z < 0.9$	10.51	16.18 (262.0)	1.63	3.14%
$0.9 < z < 1.2$	14.64	3.01 (142.8)	1.882	3.28%
$1.2 < z < 1.5$	17.48	0.16 (57.64)	2.134	-

**Table 1.** Statistical properties of the CSST spec- $z$  (photo- $z$ ) galaxy surveys in five redshift bins over a sky coverage of  $17,500 \text{ deg}^2$ . Values in parentheses refer to the photo- $z$  sample. The galaxy bias is modeled as  $b_g(z) = 1 + 0.84z$  for both surveys [52]. The error prediction of the  $\beta$  parameter in the lens redshift bin comes from [53]. The intrinsic shape noise  $\sigma_\gamma$  is set to be 0.2 [54].

Due to the large and overlapping sky coverage of the CSST photometric and spectroscopic surveys, it will be possible to jointly probe the growth and geometry of the Universe using multiple cosmological observables. These include weak gravitational lensing [51, 54, 55], cluster number counts [56, 57], the Alcock Paczynski (AP) effect [58], RSD effect [51, 59], baryon acoustic oscillations (BAO) [60, 61], among others. The CSST is therefore expected to serve as a powerful instrument for investigating both the expansion history of the Universe and the growth of cosmic structures. In particular, by combining various cosmological probes within the CSST survey, one can obtain more robust and precise constraints on fundamental cosmological parameters, effectively breaking degeneracies that arise when using individual probes alone [41, 51].

Similar to [62], in this work we make use of redshift distribution of the mock galaxy catalogs for the CSST surveys provided by [51, 63], which are based on the COSMOS galaxy catalog [64, 65] and the  $z$ COSMOS spectroscopic samples [66, 67]. [63] constructed two photometric-redshift (photo- $z$ ,  $z_p$ ) samples using a sub-set (95% and 58%) of the COSMOS catalog, with photometric redshift uncertainties respectively being  $\sigma_{z_p} = 0.025(1 + z_p)$  and  $\sigma_{z_p} = 0.05(1 + z_p)$ . The left panel of figure 1 shows the redshift distributions of galaxies in the range  $0 < z < 1.5$  for these two photo- $z$  samples, and in our analysis, we adopt the photo- $z$  sample with  $\sigma_{z_p} = 0.025(1 + z_p)$  as the fiducial mock configuration.

We also consider the galaxy redshift distribution of the CSST slitless spectroscopic (spec- $z$ ,  $z_s$ ) survey. Following [62], we extract from  $z$ COSMOS a sub-sample with robust redshift measurements, representing about 80 per cent of the full sample and covering  $0 < z \leq 1.5$ . Its normalized spectroscopic redshift distribution (right panel of figure 1) exhibits a steep decline beyond  $z = 1.0$ . Moreover, we account for redshift uncertainties arising from the limited spectroscopic resolution of CSST slitless spectroscopy. Our baseline model incorporates the error parameterization  $\sigma_{z_s} = 0.002(1 + z_s)$  [68] and a redshift success rate of the form  $f_{\text{eff}}^z = f_{\text{eff}}^0(1 + z_s)$  [69], where  $f_{\text{eff}}^0$  denotes the success fraction at  $z = 0$ . We adopt  $f_{\text{eff}}^0 = 0.5$  as our fiducial choice and show the corresponding comoving volume number density of spec- $z$  galaxy as the solid line in the right panel of figure 1.

These photo- $z$  and spec- $z$  mock samples provide a consistent framework to evaluate the CSST survey performance for weak lensing and galaxy clustering analyses. The redshift binning scheme, comoving survey volume, galaxy number density, galaxy bias and the corresponding error prediction of  $\beta$  for each redshift bin are summarized in Table 1.

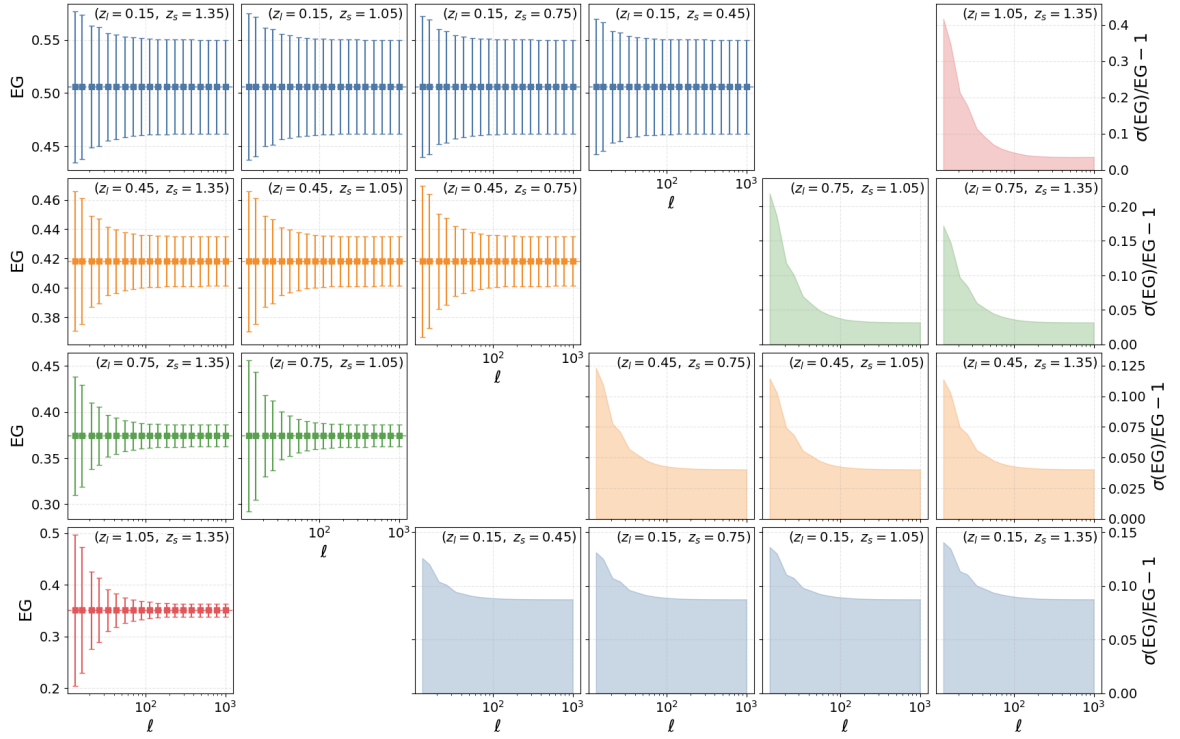


**Figure 2.** Forecasted  $E_G$  measurements in harmonic space. The upper panel shows  $E_G(\ell)$  for different combinations of lens and source bins, with error bars denoting Gaussian uncertainties. The lower panel presents the relative statistical uncertainty,  $\sigma(E_G)/E_G - 1$ , as a function of multipole  $\ell$ .

## 4 Results

### 4.1 $E_G$ predictions

We present predictions for the  $E_G$  statistic based on the mock CSST redshift distributions detailed in Section 3. Figure 2 summarizes the results. The top left panels show  $E_G(\ell)$  for various combinations of lens and source redshift bins, while the lower right panels display the relative statistical uncertainty,  $\sigma(E_G)/E_G$ , as a function of multipole  $\ell$  across 20 log-spaced bins between  $\ell = 10$  and  $\ell = 1000$ .

Our forecasts indicate that few-percent level precision on  $E_G$  is achievable over a wide range of angular scales and lens-source redshift pairs. The constraints exhibit a distinct scale dependence: at large scales ( $\ell < 100$ ), cosmic variance dominates, leading to larger uncertainties. At smaller scales ( $\ell > 100$ ), the precision improves significantly, with constraints reaching  $\sim 4\%$  across various lens redshift bins. This scale-dependent behavior can be understood by comparing with the  $\beta$  constraints in Table 1. At small scales, the  $E_G$  constraints are predominantly limited by the precision on  $\beta$ , which explains the flattening of the  $E_G$  uncertainty curves in this regime.

To obtain a scale-independent  $E_G$  constraint, we combine the  $E_G(\ell)$  measurements across different multipoles using equation (2.17). In this process, we adopt the simplifying assumption that, for a given lens redshift bin, we treat all available source redshift bins as a single combined source sample to maximize the lensing signal. The resulting integrated  $E_G$  constraints as a function of the lens redshift are shown in the left panel of figure 3. The predicted

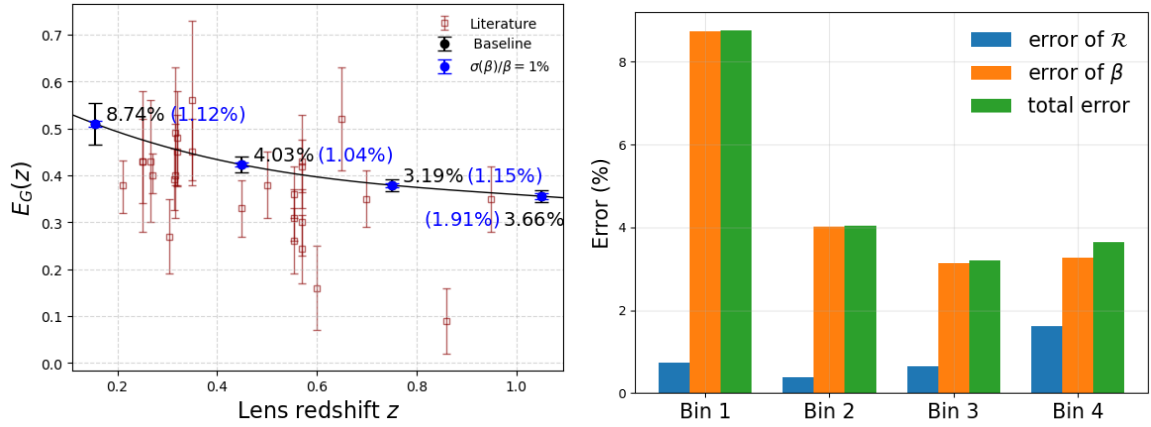


**Figure 3.** *Left:* redshift evolution of the  $E_G$  statistic after combining all source bins for each lens bin. Blue points with error bars show the results assuming  $\sigma(\beta)/\beta = 1\%$ . Percentile numbers beside data points represent the fractional errors of  $E_G$ . Data represented by hollow red squares show current  $E_G$  measurements from the literature collected in table 2. For clarity and compactness of the figure, the data point at  $z = 1.5$  in table 2 ( $E_G = 0.30 \pm 0.05$  [35]) is not shown. *Right:* Fractional error contributions to the  $E_G$  estimator. The bars show the total statistical uncertainty, the error from the measurement of the structure growth rate  $\beta$ , and the combined contributions from all other sources.

$z$	$E_G$	Ref	$z$	$E_G$	Ref
0.21	$0.38^{+0.052}_{-0.061}$	[28]	0.50	$0.38 \pm 0.07$	[31]
0.25	$0.43 \pm 0.09$	[25]	0.554	$0.26 \pm 0.07$	[27]
0.25	$0.43 \pm 0.15$	[31]	0.555	$0.36^{+0.06}_{-0.05}$	[33]
0.267	$0.43 \pm 0.13$	[27]	0.555	$0.31^{+0.06}_{-0.05}$	[32]
0.27	$0.40^{+0.046}_{-0.038}$	[28]	0.57	$0.30 \pm 0.07$	[24]
0.305	$0.27 \pm 0.08$	[27]	0.57	$0.42 \pm 0.056$	[26]
0.315	$0.392 \pm 0.065$	[29]	0.57	$0.43 \pm 0.10$	[30]
0.316	$0.40^{+0.11}_{-0.09}$	[33]	0.57	$0.243 \pm 0.073$	[34]
0.316	$0.49^{+0.14}_{-0.11}$	[32]	0.60	$0.16 \pm 0.09$	[36]
0.32	$0.48 \pm 0.10$	[24]	0.65	$0.52 \pm 0.11$	[31]
0.32	$0.45^{+0.080}_{-0.073}$	[28]	0.70	$0.35 \pm 0.06$	[31]
0.35	$0.56 \pm 0.17$	[31]	0.86	$0.09 \pm 0.07$	[36]
0.35	$0.45 \pm 0.07$	[25]	0.95	$0.35 \pm 0.07$	[31]
0.45	$0.33 \pm 0.06$	[25]	1.50	$0.30 \pm 0.05$	[35]

**Table 2.** Compilation of  $E_G$  measurements from the literature, ordered by redshift.

$E_G$  measurements can reach 3% – 9% over the lens redshift range  $0 < z < 1.2$  — a factor of several to an order of magnitude improvement over current observations. These results demonstrate that CSST will be a highly competitive facility for future  $E_G$  studies across a broad range of scales and redshifts [70–74].

As anticipated, the total uncertainty on  $E_G$  is dominated by the limited precision in

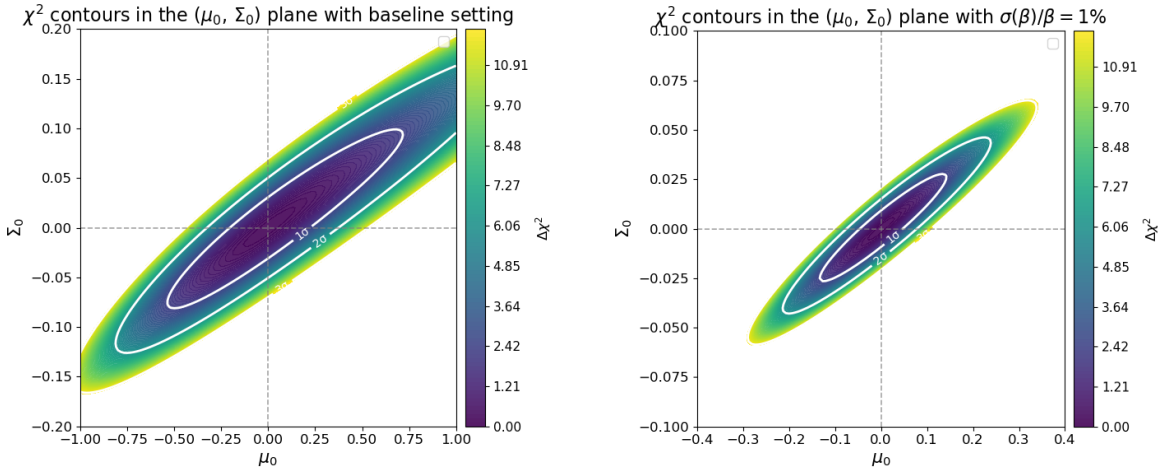


**Figure 4.**  $\chi^2$  confidence contours in the  $(\mu_0, \Sigma_0)$  plane, derived from the forecasted  $E_G$  measurements. The contours represent the 68% and 95% joint confidence regions. *Left:* Baseline result.  $\mu_0 = 0^{+0.483}_{-0.324}$ ,  $\Sigma_0 = 0^{+0.064}_{-0.052}$ . *Right:* The case where  $\sigma(\beta)/\beta$  is set to 1%.  $\mu_0 = 0^{+0.0908}_{-0.0921}$ ,  $\Sigma_0 = 0^{+0.0177}_{-0.0184}$ .

determining  $\beta$  through the RSD effect. This is explicitly demonstrated in the right panel of figure 3, which compares the fractional error contributions from the ratio  $\mathcal{R} = C^{g\kappa}/C^{gg}$  and from  $\beta$ . Consequently, improving the overall  $E_G$  precision hinges primarily on obtaining tighter constraints on  $\beta$ . This conclusion holds true for the current  $E_G$  detections as well, and is supported by the findings of [75], who achieved 6 – 11.3% precision of  $E_G$  measurements by obtaining improved  $\beta$  constraints through a model-independent Gaussian process reconstruction that combined multiple literature measurements. To illustrate the potential gain, we also show in the left panel of figure 3 a forecast scenario where  $\beta$  is assumed to be known with 1% precision at all redshifts. In this idealised case, percent-level precision on  $E_G$  becomes achievable across a wide redshift range.

## 4.2 Constraints on modified gravity

This redshift-dependent summary of  $E_G$  predictions highlights the overall constraining power of CSST across  $0 < z < 1.5$ , and provides a convenient tomographic view of the  $E_G$  statistic for testing modified-gravity scenarios. To translate the forecasted  $E_G$  measurements into anticipated constraints on modified gravity, we evaluate the likelihood of the phenomenological parameters  $(\mu_0, \Sigma_0)$  entering the  $\mu - \Sigma$  parametrization described in section 2.3. Figure 4 shows the resulting  $\chi^2$  contours in the  $(\mu_0, \Sigma_0)$  plane.

We first note a strong degeneracy between  $\mu_0$  and  $\Sigma_0$ , as expected from their respective roles in the denominator and numerator of equation (2.20). The forecast constraints for the CSST baseline configuration are shown in the left panel of figure 4. While  $\mu_0$  can be constrained at the level of 30 – 50%, the precision on  $\Sigma_0$  is significantly higher, reaching 5%. This indicates that  $E_G$  is more sensitive to  $\Sigma_0$  than to  $\mu_0$ , likely because the dependence on  $\Sigma_0$  in the numerator of equation (2.20) is direct and linear, whereas the dependence on  $\mu_0$  in the denominator is indirect and nonlinear. These baseline forecasts suggest that CSST will deliver competitive constraints on modified gravity parameters [21, 22, 74, 76].

This potential is further underscored by an idealized scenario with  $\sigma(\beta)/\beta = 1\%$  (right panel of figure 4), which yields 5 times tighter constraints on both parameters. In particular,

by leveraging improved  $\beta$  measurements—anticipated at the percent level—from spectroscopic surveys like MUST [76] and WST [77], it becomes feasible to achieve percent-level constraints on  $\Sigma_0$ , the parameter associated with the effective gravitational constant of the Weyl potential. Such a measurement would provide a stringent direct test of the strength of gravity on cosmological scales, offering a critical benchmark to distinguish GR from modified gravity models.

## 5 Conclusion

In this study, we have systematically forecast the potential of the CSST survey to measure the  $E_G$  statistic, a powerful multi-tracer test of gravitational physics on cosmological scales. By adopting redshift distributions of realistic mock spectroscopic and photometric galaxy samples, we developed a comprehensive harmonic-space covariance framework that fully accounts for the cross-correlation between galaxy–galaxy lensing and galaxy clustering observables.

Our analysis yields several key quantitative outcomes:

- CSST will achieve a few-percent level precision on  $E_G$  over a wide range of angular scales, with constraints reaching  $\sim 4\%$  at  $\ell > 100$  across various lens redshift bins. By compressing information of various scales and source redshift bins, the predicted scale-independent  $E_G$  measurements can reach  $3\% - 9\%$  at  $0 < z < 1.2$  — a factor of several to an order of magnitude improvement over current observations.
- Within the  $\mu - \Sigma$  parametrization of modified gravity, CSST can constrain  $\Sigma_0$ —the parameter associated with the effective gravitational constant of the Weyl potential—to  $\sim 5\%$ , while  $\mu_0$  is constrained at the  $30 - 50\%$  level.
- The dominant source of uncertainty in  $E_G$  originates from the RSD parameter  $\beta$ , whose precision limits the overall constraining power. If future spectroscopic surveys improve  $\beta$  constraints to the  $1\%$  level,  $E_G$  can be also measured at the percent-level over a wide redshift range, and both  $\mu_0$  and  $\Sigma_0$  could be constrained about five times more tightly, with  $\Sigma_0$  approaching percent-level precision.

These results confirm that CSST will serve as a highly competitive Stage-IV facility for tomographic tests of gravity. The  $E_G$  statistic, benefiting from the inherent cancellation of cosmic variance and independence from galaxy bias and  $\sigma_8$ , offers a robust and model-independent diagnostic for deviations from GR. Our forecasts further highlight the critical synergy between photometric weak lensing surveys and high-precision spectroscopic campaigns: improvements in  $\beta$  determination directly and substantially enhance the  $E_G$  constraining power.

Looking ahead, the methodology and baseline predictions presented here will provide a ready framework for the cosmological interpretation of real CSST data. Subsequent analyses will need to incorporate more realistic treatments of photometric redshift errors, intrinsic alignments, lensing magnification and higher-order systematics [22]. In combination with contemporaneous surveys such as Euclid [37], LSST [38], DESI [39], MUST [76] and WST [77], CSST is poised to deliver transformative constraints on modified gravity models and advance our understanding of cosmic acceleration.

## Acknowledgments

We thank Zhejie Ding, Yan Gong for helpful discussions. Y.Z. acknowledges the supports from the National SKA Program of China (2025SKA0150104) and the National Natural Science Foundation of China (NFSC) through grant 12203107.

## References

- [1] A. G. Riess, A. V. Filippenko, P. Challis, A. Clocchiatti, A. Diercks, P. M. Garnavich et al., *Observational Evidence from Supernovae for an Accelerating Universe and a Cosmological Constant*, *AJ* **116** (Sept., 1998) 1009–1038, [[astro-ph/9805201](#)].
- [2] S. Perlmutter, G. Aldering, G. Goldhaber, R. A. Knop, P. Nugent, P. G. Castro et al., *Measurements of  $\Omega$  and  $\Lambda$  from 42 High-Redshift Supernovae*, *ApJ* **517** (June, 1999) 565–586, [[astro-ph/9812133](#)].
- [3] E. Di Valentino, O. Mena, S. Pan, L. Visinelli, W. Yang, A. Melchiorri et al., *In the realm of the Hubble tension-a review of solutions*, *Classical and Quantum Gravity* **38** (July, 2021) 153001, [[2103.01183](#)].
- [4] L. Verde, N. Schöneberg and H. Gil-Marín, *A Tale of Many  $H_0$* , *ARA&A* **62** (Sept., 2024) 287–331, [[2311.13305](#)].
- [5] H. Miyatake, S. Sugiyama, M. Takada, T. Nishimichi, X. Li, M. Shirasaki et al., *Hyper Suprime-Cam Year 3 results: Cosmology from galaxy clustering and weak lensing with HSC and SDSS using the emulator based halo model*, *PRD* **108** (Dec., 2023) 123517, [[2304.00704](#)].
- [6] M. Abdul Karim, J. Aguilar, S. Ahlen, S. Alam, L. Allen, C. A. Prieto et al., *DESI DR2 results. II. Measurements of baryon acoustic oscillations and cosmological constraints*, *PRD* **112** (Oct., 2025) 083515, [[2503.14738](#)].
- [7] DES Collaboration, T. M. C. Abbott, M. Adamow, M. Aguena, A. Alarcon, S. S. Allam et al., *Dark Energy Survey Year 6 Results: Cosmological Constraints from Galaxy Clustering and Weak Lensing*, *arXiv e-prints* (Jan., 2026) arXiv:2601.14559, [[2601.14559](#)].
- [8] G. Hinshaw, D. Larson, E. Komatsu, D. N. Spergel, C. L. Bennett, J. Dunkley et al., *Nine-year Wilkinson Microwave Anisotropy Probe (WMAP) Observations: Cosmological Parameter Results*, *ApJS* **208** (Oct., 2013) 19, [[1212.5226](#)].
- [9] Planck Collaboration, N. Aghanim, Y. Akrami, M. Ashdown, J. Aumont, C. Baccigalupi et al., *Planck 2018 results. VI. Cosmological parameters*, *Astron. Astrophys.* **641** (Sept., 2020) A6, [[1807.06209](#)].
- [10] S. Alam, M. Aubert, S. Avila, C. Balland, J. E. Bautista, M. A. Bershady et al., *Completed SDSS-IV extended Baryon Oscillation Spectroscopic Survey: Cosmological implications from two decades of spectroscopic surveys at the Apache Point Observatory*, *PRD* **103** (Apr., 2021) 083533, [[2007.08991](#)].
- [11] E. Calabrese, J. C. Hill, H. T. Jense, A. La Posta, I. Abril-Cabezas, G. E. Addison et al., *The Atacama Cosmology Telescope: DR6 constraints on extended cosmological models*, *JCAP* **2025** (Nov., 2025) 063, [[2503.14454](#)].
- [12] A. H. Wright, B. Stölzner, M. Asgari, M. Bilicki, B. Giblin, C. Heymans et al., *KiDS-Legacy: Cosmological constraints from cosmic shear with the complete Kilo-Degree Survey*, *Astron. Astrophys.* **703** (Nov., 2025) A158, [[2503.19441](#)].
- [13] E. Camphuis, W. Quan, L. Balkenhol, A. R. Khalife, F. Ge, F. Guidi et al., *SPT-3G D1: CMB temperature and polarization power spectra and cosmology from 2019 and 2020 observations of the SPT-3G Main field*, *arXiv e-prints* (June, 2025) arXiv:2506.20707, [[2506.20707](#)].

[14] D. H. Weinberg, M. J. Mortonson, D. J. Eisenstein, C. Hirata, A. G. Riess and E. Rozo, *Observational probes of cosmic acceleration*, *Physics reports* **530** (Sept., 2013) 87–255, [[1201.2434](#)].

[15] I. Zlatev, L. Wang and P. J. Steinhardt, *Quintessence, Cosmic Coincidence, and the Cosmological Constant*, *PRL* **82** (Feb., 1999) 896–899, [[astro-ph/9807002](#)].

[16] J. Martin, *Everything you always wanted to know about the cosmological constant problem (but were afraid to ask)*, *Comptes Rendus Physique* **13** (July, 2012) 566–665, [[1205.3365](#)].

[17] A. Joyce, B. Jain, J. Khoury and M. Trodden, *Beyond the cosmological standard model*, *Physics reports* **568** (Mar., 2015) 1–98, [[1407.0059](#)].

[18] D. H. Weinberg, M. J. Mortonson, D. J. Eisenstein, C. Hirata, A. G. Riess and E. Rozo, *Observational probes of cosmic acceleration*, *Physics reports* **530** (Sept., 2013) 87–255, [[1201.2434](#)].

[19] A. Joyce, L. Lombriser and F. Schmidt, *Dark Energy Versus Modified Gravity*, *Annual Review of Nuclear and Particle Science* **66** (Oct., 2016) 95–122, [[1601.06133](#)].

[20] K. Koyama, *Cosmological tests of modified gravity*, *Reports on Progress in Physics* **79** (Apr., 2016) 046902, [[1504.04623](#)].

[21] S. Alam, C. Arnold, A. Aviles, R. Bean, Y.-C. Cai, M. Cautun et al., *Towards testing the theory of gravity with DESI: summary statistics, model predictions and future simulation requirements*, *JCAP* **2021** (Nov., 2021) 050, [[2011.05771](#)].

[22] Euclid Collaboration, N. Frusciante, M. Martinelli, L. Lombriser, A. Silvestri, M. Archidiacono et al., *Euclid preparation. Review of forecast constraints on dark energy and modified gravity*, *arXiv e-prints* (Dec., 2025) arXiv:2512.09748, [[2512.09748](#)].

[23] P. Zhang, M. Liguori, R. Bean and S. Dodelson, *Probing Gravity at Cosmological Scales by Measurements which Test the Relationship between Gravitational Lensing and Matter Overdensity*, *PRL* **99** (Oct., 2007) 141302, [[0704.1932](#)].

[24] C. Blake, S. Joudaki, C. Heymans, A. Choi, T. Erben, J. Harnois-Deraps et al., *RCSLenS: testing gravitational physics through the cross-correlation of weak lensing and large-scale structure*, *MNRAS* **456** (Mar., 2016) 2806–2828, [[1507.03086](#)].

[25] C. Blake, A. Amon, M. Asgari, M. Bilicki, A. Dvornik, T. Erben et al., *Testing gravity using galaxy-galaxy lensing and clustering amplitudes in KiDS-1000, BOSS, and 2dFLenS*, *Astron. Astrophys.* **642** (Oct., 2020) A158, [[2005.14351](#)].

[26] S. Alam, H. Miyatake, S. More, S. Ho and R. Mandelbaum, *Testing gravity on large scales by combining weak lensing with galaxy clustering using CFHTLenS and BOSS CMASS*, *MNRAS* **465** (Mar., 2017) 4853–4865, [[1610.09410](#)].

[27] A. Amon, C. Blake, C. Heymans, C. D. Leonard, M. Asgari, M. Bilicki et al., *KiDS+2dFLenS+GAMA: testing the cosmological model with the  $E_G$  statistic*, *MNRAS* **479** (Sept., 2018) 3422–3437, [[1711.10999](#)].

[28] S. Singh, S. Alam, R. Mandelbaum, U. Seljak, S. Rodriguez-Torres and S. Ho, *Probing gravity with a joint analysis of galaxy and CMB lensing and SDSS spectroscopy*, *MNRAS* **482** (Jan., 2019) 785–806, [[1803.08915](#)].

[29] R. Reyes, R. Mandelbaum, U. Seljak, T. Baldauf, J. E. Gunn, L. Lombriser et al., *Confirmation of general relativity on large scales from weak lensing and galaxy velocities*, *Nature* **464** (Mar., 2010) 256–258, [[1003.2185](#)].

[30] E. Jullo, S. de la Torre, M.-C. Cousinou, S. Escoffier, C. Giocoli, R. B. Metcalf et al., *Testing gravity with galaxy-galaxy lensing and redshift-space distortions using CFHT-Stripe 82, CFHTLenS, and BOSS CMASS datasets*, *Astron. Astrophys.* **627** (July, 2019) A137, [[1903.07160](#)].

[31] S. J. Rauhut, C. Blake, U. Andrade, H. E. Noriega, J. Aguilar, S. Ahlen et al., *Testing gravitational physics by combining DESI DR1 and weak lensing datasets using the E\_G estimator*, *The Open Journal of Astrophysics* **8** (Oct., 2025) 149, [[2507.16098](#)].

[32] L. Wenzl, R. An, N. Battaglia, R. Bean, E. Calabrese, S.-F. Chen et al., *Atacama Cosmology Telescope: DR6 gravitational lensing and SDSS BOSS cross-correlation measurement and constraints on gravity with the EG statistic*, *PRD* **111** (Feb., 2025) 043535, [[2405.12795](#)].

[33] L. Wenzl, R. Bean, S.-F. Chen, G. S. Farren, M. S. Madhavacheril, G. A. Marques et al., *Constraining gravity with a new precision EG estimator using Planck + SDSS BOSS data*, *PRD* **109** (Apr., 2024) 083540, [[2401.12971](#)].

[34] A. R. Pullen, S. Alam, S. He and S. Ho, *Constraining gravity at the largest scales through CMB lensing and galaxy velocities*, *MNRAS* **460** (Aug., 2016) 4098–4108, [[1511.04457](#)].

[35] Y. Zhang, A. R. Pullen, S. Alam, S. Singh, E. Burtin, C.-H. Chuang et al., *Testing general relativity on cosmological scales at redshift  $z \sim 1.5$  with quasar and CMB lensing*, *MNRAS* **501** (Feb., 2021) 1013–1027, [[2007.12607](#)].

[36] S. de la Torre, E. Jullo, C. Giocoli, A. Pezzotta, J. Bel, B. R. Granett et al., *The VIMOS Public Extragalactic Redshift Survey (VIPERS). Gravity test from the combination of redshift-space distortions and galaxy-galaxy lensing at  $0.5 < z < 1.2$* , *Astron. Astrophys.* **608** (Dec., 2017) A44, [[1612.05647](#)].

[37] R. Laureijs, J. Amiaux, S. Arduini, J. Augu  res, J. Brinchmann, R. Cole et al., *Euclid Definition Study Report*, *ArXiv e-prints* (Oct., 2011) , [[1110.3193](#)].

[38] LSST Dark Energy Science Collaboration, *Large Synoptic Survey Telescope: Dark Energy Science Collaboration*, *arXiv e-prints* (Nov., 2012) arXiv:1211.0310, [[1211.0310](#)].

[39] DESI Collaboration, A. Aghamousa, J. Aguilar, S. Ahlen, S. Alam, L. E. Allen et al., *The DESI Experiment Part I: Science, Targeting, and Survey Design*, *arXiv e-prints* (Oct., 2016) arXiv:1611.00036, [[1611.00036](#)].

[40] M. Takada, R. S. Ellis, M. Chiba, J. E. Greene, H. Aihara, N. Arimoto et al., *Extragalactic science, cosmology, and Galactic archaeology with the Subaru Prime Focus Spectrograph*, *PASJ* **66** (Feb., 2014) R1, [[1206.0737](#)].

[41] CSST Collaboration, Y. Gong, H. Miao, H. Zhan, Z.-Y. Li, J. Shangguan et al., *Introduction to the Chinese Space Station Survey Telescope (CSST)*, *Science China Physics, Mechanics, and Astronomy* **69** (Jan., 2026) 239501.

[42] G.-B. Zhao, T. Giannantonio, L. Pogosian, A. Silvestri, D. J. Bacon, K. Koyama et al., *Probing modifications of general relativity using current cosmological observations*, *PRD* **81** (May, 2010) 103510, [[1003.0001](#)].

[43] E. V. Linder, *Cosmic growth history and expansion history*, *PRD* **72** (Aug., 2005) 043529, [[arXiv:astro-ph/0507263](#)].

[44] R. Laureijs, J. Amiaux, S. Arduini and et al., *Euclid definition study report*, *arXiv preprint arXiv:1110.3193* (2011) .

[45]  . Ivezi , S. M. Kahn, J. A. Tyson and et al., *Lsst: From science drivers to reference design and anticipated data products*, *The Astrophysical Journal* **873** (2019) 111.

[46] Y. Shi, P. Zhang, Z. Sun and Y. Wang, *Accurate kappa reconstruction algorithm for masked shear catalog*, *PRD* **109** (June, 2024) 123530, [[2311.00316](#)].

[47] A. R. Pullen, S. Alam, S. He and S. Ho, *Constraining gravity at the largest scales through CMB lensing and galaxy velocities*, *MNRAS* **460** (Aug., 2016) 4098–4108, [[1511.04457](#)].

[48] N. E. Chisari, D. Alonso, E. Krause, C. D. Leonard, P. Bull, J. Neveu et al., *Core Cosmology Library: Precision Cosmological Predictions for LSST*, *ApJS* **242** (May, 2019) 2, [[1812.05995](#)].

[49] F. Simpson, C. Heymans, D. Parkinson, C. Blake, M. Kilbinger, J. Benjamin et al., *CFHTLenS: testing the laws of gravity with tomographic weak lensing and redshift-space distortions*, *MNRAS* **429** (Mar., 2013) 2249–2263, [[1212.3339](#)].

[50] Planck Collaboration, P. A. R. Ade, N. Aghanim, M. Arnaud, M. Ashdown, J. Aumont et al., *Planck 2015 results. XIV. Dark energy and modified gravity*, *Astron. Astrophys.* **594** (Sept., 2016) A14, [[1502.01590](#)].

[51] Y. Gong, X. Liu, Y. Cao, X. Chen, Z. Fan, R. Li et al., *Cosmology from the Chinese Space Station Optical Survey (CSS-OS)*, *ApJ* **883** (Oct., 2019) 203, [[1901.04634](#)].

[52] Z. Ding, Y. Yu and P. Zhang, *Fisher forecast for the BAO measurements from the CSST spectroscopic and photometric galaxy clustering*, *MNRAS* **527** (Jan., 2024) 3728–3740, [[2305.00404](#)].

[53] Z. Li and Y. Zheng, *Cosmological gains from the multi-tracer analysis between RSD and kSZ effects of next generation surveys*, *in preparation* (2025) .

[54] H. Lin, Y. Gong, X. Chen, K. C. Chan, Z. Fan and H. Zhan, *Forecast of neutrino cosmology from the CSST photometric galaxy clustering and cosmic shear surveys*, *MNRAS* **515** (Oct., 2022) 5743–5757, [[2203.11429](#)].

[55] Q. Xiong, Y. Gong, X. Zhou, H. Lin, F. Deng, Z. Li et al., *Exploring Cosmological Constraints of the Weak Gravitational Lensing and Galaxy Clustering Joint Analysis in the CSST Photometric Survey*, *ApJ* **985** (May, 2025) 131, [[2410.19388](#)].

[56] Y. Zhang, M. Chen, Z. Wen and W. Fang, *Constraints on Dark Energy from the CSST Galaxy Clusters*, *Research in Astronomy and Astrophysics* **23** (Apr., 2023) 045011, [[2302.05010](#)].

[57] M. Chen, W. Fang, Y. Zhang, Z. Wen and W. Cui, *Constraining the neutrino mass with the CSST galaxy clusters*, *PRD* **112** (Sept., 2025) 063506, [[2411.02752](#)].

[58] L. Xiao, Z. Huang, Y. Zheng, X. Wang and X.-D. Li, *Tomographic Alcock-Paczynski method with redshift errors*, *MNRAS* **518** (Feb., 2023) 6253–6261, [[2210.12671](#)].

[59] H. Miao, Y. Gong, X. Chen, Z. Huang, X.-D. Li and H. Zhan, *Cosmological constraint precision of photometric and spectroscopic multi-probe surveys of China Space Station Telescope (CSST)*, *MNRAS* **519** (Feb., 2023) 1132–1148, [[2206.09822](#)].

[60] Z. Ding, Y. Yu and P. Zhang, *Fisher forecast for the BAO measurements from the CSST spectroscopic and photometric galaxy clustering*, *MNRAS* **527** (Jan., 2024) 3728–3740, [[2305.00404](#)].

[61] H. Miao, Y. Gong, X. Chen, Z. Huang, X.-D. Li and H. Zhan, *Forecasting the BAO measurements of the CSST galaxy and AGN spectroscopic surveys*, *MNRAS* **531** (July, 2024) 3991–4005, [[2311.16903](#)].

[62] Z. Ding, Y. Yu and P. Zhang, *Fisher forecast for the BAO measurements from the CSST spectroscopic and photometric galaxy clustering*, *MNRAS* **527** (Jan., 2024) 3728–3740, [[2305.00404](#)].

[63] S. Cao, X. Zhang, Y. Gong and X. Chen, *Photometric redshift simulation and mock catalogs for CSST galaxy surveys*, *Research in Astronomy and Astrophysics* **18** (June, 2018) 064, [[1805.08170](#)].

[64] P. Capak, H. Aussel, M. Ajiki, H. J. McCracken, B. Mobasher, N. Scoville et al., *The First Release COSMOS Optical and Near-IR Data and Catalog*, *ApJS* **172** (Sept., 2007) 99–116, [[0704.2430](#)].

[65] O. Ilbert, P. Capak, M. Salvato, H. Aussel, H. J. McCracken, D. B. Sanders et al., *Cosmos Photometric Redshifts with 30-Bands for 2-deg<sup>2</sup>*, *ApJ* **690** (Jan., 2009) 1236–1249, [[0809.2101](#)].

[66] S. J. Lilly, O. Le Fèvre, A. Renzini, G. Zamorani, M. Scoville, T. Contini et al., *zCOSMOS: A Large VLT/VIMOS Redshift Survey Covering  $0 < z < 3$  in the COSMOS Field*, *ApJS* **172** (Sept., 2007) 70–85, [[astro-ph/0612291](#)].

[67] S. J. Lilly, V. Le Brun, C. Maier, V. Mainieri, M. Mignoli, M. Scoville et al., *The zCOSMOS 10k-Bright Spectroscopic Sample*, *ApJS* **184** (Oct., 2009) 218–229.

[68] Y. Gong, X. Liu, Y. Cao, X. Chen, Z. Fan, R. Li et al., *Cosmology from the Chinese Space Station Optical Survey (CSS-OS)*, *ApJ* **883** (Oct., 2019) 203, [[1901.04634](#)].

[69] Y. Wang, W. Percival, A. Cimatti, P. Mukherjee, L. Guzzo, C. M. Baugh et al., *Designing a space-based galaxy redshift survey to probe dark energy*, *MNRAS* **409** (Dec., 2010) 737–749, [[1006.3517](#)].

[70] A. R. Pullen, S. Alam and S. Ho, *Probing gravity at large scales through CMB lensing*, *MNRAS* **449** (June, 2015) 4326–4335, [[1412.4454](#)].

[71] A. Pourtsidou, *Testing gravity at large scales with H I intensity mapping*, *MNRAS* **461** (Sept., 2016) 1457–1464, [[1511.05927](#)].

[72] M. M. Abidi, C. Bonvin, M. Jalilvand and M. Kunz, *Model-independent test for gravity using intensity mapping and galaxy clustering*, *PRD* **107** (Mar., 2023) 063514, [[2208.10419](#)].

[73] R. Patki, N. Battaglia and R. Bean, *Probing Gravity at Large Scales with kSZ-Reconstructed Velocities and CMB Lensing*, *arXiv e-prints* (Oct., 2025) arXiv:2510.27605, [[2510.27605](#)].

[74] C. D. Leonard, S. Alam, R. Mandelbaum, M. M. Rau, S. Singh, C. M. A. Zanoletti et al., *Towards testing gravity with LSST using  $E_G$* , *arXiv e-prints* (Nov., 2025) arXiv:2511.19194, [[2511.19194](#)].

[75] N. Grimm, C. Bonvin and I. Tuterus, *Testing General Relativity through the EG Statistic Using the Weyl Potential and Galaxy Velocities*, *PRL* **133** (Nov., 2024) 211004, [[2403.13709](#)].

[76] C. Zhao, S. Huang, M. He, P. Montero-Camacho, Y. Liu, P. Renard et al., *MULTiplexed Survey Telescope: Perspectives for Large-Scale Structure Cosmology in the Era of Stage-V Spectroscopic Survey*, *arXiv e-prints* (Nov., 2024) arXiv:2411.07970, [[2411.07970](#)].

[77] V. Mainieri, R. I. Anderson, J. Brinchmann, A. Cimatti, R. S. Ellis, V. Hill et al., *The Wide-field Spectroscopic Telescope (WST) Science White Paper*, *arXiv e-prints* (Mar., 2024) arXiv:2403.05398, [[2403.05398](#)].